The Astronomical Journal, 132:1910–1917, 2006 November
© 2006. The American Astronomical Society. All rights reserved. Printed in U.S.A.

HD 131861, A DOUBLE-LINE SPECTROSCOPIC TRIPLE SYSTEM

Francis C. Fekel[1] and Gregory W. Henry
Center of Excellence in Information Systems, Tennessee State University, 3500 John A. Merritt Boulevard, Box 9501, Nashville, TN 37209; fekel@evans.tsuniv.edu, henry@schwab.tsuniv.edu

D. J. Barlow
Department of Physics and Astronomy, University of Victoria, Victoria, BC V8W 3P6, Canada; barlow@uvic.ca

and

D. Pourbaix[2]
Institut d'Astronomie et d'Astrophysique, Université Libre de Bruxelles, C.P. 226, Boulevard du Triomphe, 1050 Brussels, Belgium; pourbaix@astro.ulb.ac.be
Received 2006 April 18; accepted 2006 July 13

ABSTRACT

Our red-wavelength spectroscopic observations of HD 131861, a previously known single-line multiple system, span 20 years. Now lines of two components, the short-period F5 V primary and G8 V secondary, have been detected. The inner orbit is circular with a period of 3.5507439 days, while the outer orbit of the system has a period of 1642 days or 4.496 yr and a relatively low eccentricity of 0.10. Analysis of the *Hipparcos* data produces a well-determined astrometric orbit for the long-period system that has an inclination of 52°. Our photometric observations show shallow primary and secondary eclipses of the short-period pair, and eclipse solutions result in an inclination of 81°. Thus, the long- and short-period orbits are not coplanar. The mass of the unseen third component is 0.7 $M_{\odot}$, corresponding to a mid-K dwarf. The total mass of the system, 3.08 $M_{\odot}$, leads to a semimajor axis of 4 AU for the outer orbit. The F5 V primary is rotating more slowly than it would if it were synchronously rotating, while the G8 V secondary may be synchronously rotating. The lithium abundance of the F5 V primary is similar to the initial lithium abundance found for Population I dwarfs and so indicates no significant dilution.

Key words: binaries: eclipsing — binaries: spectroscopic — stars: fundamental parameters

Online material: machine-readable table

1. INTRODUCTION

In several areas near the north Galactic pole Heard (1965) carried out a spectroscopic survey of 55 stars, which included HD 131861 = HIP 72939 ($\alpha = 14^{h}54^{m}24\overset{s}{.}5$, $\delta = 45°17'55\overset{''}{.}7$ [J2000], $V = 7.9$ mag). From 20 radial velocities obtained at David Dunlap Observatory (DDO) he discovered the star to be a spectroscopic binary and found a preliminary orbital period of 3.55 days. He also classified the star as F5 V. Soon afterward, using 42 radial velocities, Heard (1966) published an improved orbit for the single-line spectroscopic binary. He determined a period of 3.55078 days and a circular orbit. About two decades later, Mayor & Mazeh (1987) included HD 131861 in a spectroscopic search for new multiple systems carried out at Haute-Provence Observatory (HPO). They observed 25 binaries with known orbits, looking for evidence of multiplicity. From 3 years of observation they found that the center-of-mass velocity of HD 131861 varied with a period of roughly 1000 days, indicating that HD 131861 is a multiple system. They also revised the period of the short-period system to 3.550758 days. In the notes section of their binary-orbit catalog Batten et al. (1989) reported that lines of the short-period secondary had been detected, a reference to our unpublished results.

Our new spectroscopic observations enable us to determine elements of both the long- and short-period orbits. Using those results, we have reanalyzed the *Hipparcos* data and obtained an astrometric orbit for the long-period system. Analysis of our photometric observations has produced eclipsing binary solutions for the short-period system. These results and other information are combined to determine some fundamental parameters of the components and also to discuss the general properties of this multiple-star system.

2. OBSERVATIONS AND REDUCTIONS

2.1. *Spectroscopy*

From 1984 March through 2005 June we obtained 64 spectrograms of HD 131861 at the Kitt Peak National Observatory (KPNO) with the coudé feed telescope, coudé spectrograph, and a Texas Instruments CCD detector. The first seven observations, obtained from 1984 through 1987, used grating D, which resulted in a wavelength range of about 90 Å and a resolution of 0.23 Å. One spectrogram was centered at 6700 Å, while all the rest were obtained at 6430 Å. From 1988 onward grating A was used, which produced spectrograms with a wavelength range of over 80 Å and a resolution of 0.21 Å. The vast majority of the grating A observations were centered at 6430 Å, while four were obtained at 6700 Å. Most of the spectra have signal-to-noise ratios (S/Ns) of 150 or better. Figure 1 shows the spectrum of HD 131861 in the 6430 Å region with several lines of the primary and secondary of the short-period orbit, components Aa and Ab, respectively, indicated.

[1] Visiting astronomer, Kitt Peak National Observatory, National Optical Astronomy Observatory. NOAO is operated by the Association of Universities for Research in Astronomy, Inc., under cooperative agreement with the National Science Foundation.
[2] Research associate, FNRS, Belgium.

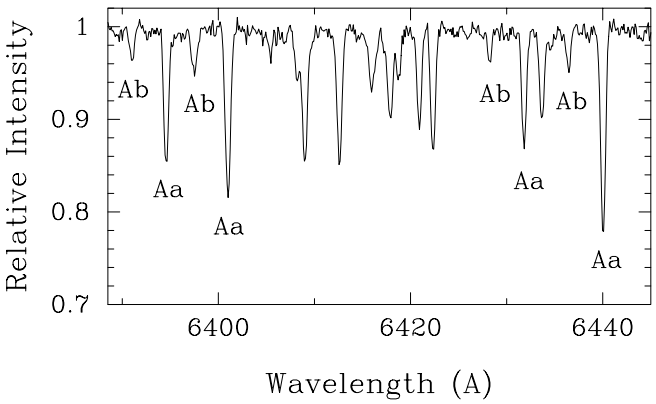

FIG. 1.—Spectrum of HD 131861 in the 6430 Å region. Several lines of components Aa and Ab are identified.

Radial velocities for the observations from 1984 through 1989 were determined with the program described by Fekel et al. (1978). Velocities from 1991 to the present were measured with the IRAF[3] cross-correlation program FXCOR (Fitzpatrick 1993). The IAU radial-velocity standards β Vir, HR 5694, and HR 7560 were used as the cross-correlation reference stars, with velocities of 4.4, 54.4, and 0.0 km s^{-1}, respectively, adopted from Scarfe et al. (1990). All of our KPNO velocities are listed in Table 1, as well as the 23 HPO velocities, which Mayor & Mazeh (1987) acquired with the Coravel radial-velocity spectrometer.

2.2. *Photometry*

We obtained our photometry of HD 131861 during the 2005 observing season with the T2 0.25 m automatic photoelectric telescope (APT) at Fairborn Observatory in the Patagonia Mountains of southern Arizona. This APT is equipped with a modified, temperature-stabilized SSP-3 photometer and photodiode detector from Optec, Inc., and acquires data through Johnson *V*, *R*, and *I* filters. The APT is programmed to measure stars in the following sequence, termed a group observation: *K, sky, C, V, C, V, C, V, C, sky, K*, where *K* is a check star, *C* is the comparison star, and *V* is the program star. A total of 2379 group observations of HD 131861 were obtained with the APT between April 5 and July 17 with HD 130044 ($V = 6.73$, $B - V = 0.292$, F0) as the comparison star and HD 130945 ($V = 5.76$, $B - V = 0.482$, F6 IVs) as the check star.

To create group means for each group observation, three variable-minus-comparison ($V - C$) and two check-minus-comparison ($K - C$) differential magnitudes in each photometric band were computed and averaged. The group means were then corrected for differential extinction with nightly extinction coefficients, transformed to the Johnson system with yearly mean transformation coefficients, and treated as single observations thereafter. The external precision of the group means, based on standard deviations for pairs of constant stars, is typically $\sim$0.006 mag on good nights with this telescope. Group mean differential magnitudes with internal standard deviations greater than 0.02 mag were discarded. The individual differential magnitudes are given in Table 2. Further details of telescope operations and data-reduction procedures can be found in Henry (1995a, 1995b).

3. SPECTROSCOPIC ORBITAL SOLUTIONS

To determine preliminary elements of the long-period orbit, the KPNO velocities of component Aa were analyzed. The period of Mayor & Mazeh (1987) was adopted for the short-period orbit, and initial orbital elements were determined from those data with BISP (Wolfe et al. 1967), a computer program that implements a slightly modified version of the Wilsing-Russell method. That orbit was then refined with SB1 (Barker et al. 1967), a program that uses differential corrections. As expected from the results of Mayor & Mazeh (1987) the systematic residuals to the SB1 orbit showed that this short-period solution contains both short- and long-period velocity variations. A sine curve was fitted to the velocity residuals for trial periods between 1000 and 3000 days with a step size of 0.5 days. For each period the sum of the squared residuals was computed, and a period of 1634.5 days, which had the smallest value of that sum, was identified as the preliminary value of the long-period orbit. Initial elements for the long-period system were then computed with BISP. Finally, taking into account the long-period velocity changes, a mass ratio of 0.62 for the short-period components, Ab and Aa, was computed from several velocity pairs and then used to determine a preliminary semiamplitude for Ab in the short-period orbit.

Differential-correction programs to determine simultaneously the short- and long-period orbits of spectroscopic triple systems have been developed at the University of Victoria by one of us (D. J. B.). The single-line versions that were used in the studies of HD 166181 (Fekel et al. 2005) and HR 5472 (Barlow & Scarfe 1991) were modified to include the secondary component of the short-period subsystem. Both the single- and double-line program versions have been used to determine several orbital solutions for HD 131861, which are described below.

With the preliminary results mentioned above, a single-line triple solution was obtained for all the KPNO Aa data in Table 1, which yielded a standard error of 0.49 km s^{-1} for an observation of unit weight. Next, a single-line triple solution was obtained for the Coravel Aa data (Table 1) with the long period fixed at the value from the KPNO Aa solution. This resulted in a standard error of 0.80 km s^{-1} for a Coravel observation of unit weight. A final single-line triple solution was obtained for the KPNO data of Ab in Table 1, again with the long period fixed at the value from the KPNO Aa solution, which yielded a standard error of 1.30 km s^{-1} for an observation of unit weight (one velocity was assigned zero weight because its residual was greater than 3 σ).

Comparing all three single-line triple solutions, we found the values of the common elements were in excellent agreement; in particular, no systematic center-of-mass velocity offset was observed, and so no zero-point corrections have been applied. All three sets of data were then combined into a double-line triple solution with weights appropriate to their scatter, as determined from the separate single-line solutions. The KPNO Aa velocities were assigned weights of 1.0, KPNO Ab velocities weights of 0.15, and HPO Aa velocities weights of 0.4. The short- and long-period elements from this solution, as well as related derived quantities, are presented in Table 3. The standard error of an observation of unit weight is 0.5 km s^{-1}. Since a time of periastron passage is undefined in a circular orbit, as recommended by Batten et al. (1989), T_0, a time of maximum radial velocity for the primary, is listed instead for the short-period orbit. In addition to the Heliocentric Julian Dates (HJD) and radial velocities of components Aa and Ab, Table 1 lists the phases of the observations in the long- and short-period orbits, the ($O - C$) or velocity residual for each component, with the calculated velocity being that for the combined long- and short-period orbits, and finally the observatory where the data were obtained. Figure 2 presents the computed velocity curves for the short-period subsystem components Aa and Ab. Each plotted velocity consists of

[3] IRAF is distributed by the National Optical Astronomy Observatory.

TABLE 1

RADIAL VELOCITIES OF HD 131861

Heliocentric Julian Date (HJD − 2,400,000)	ϕ_L	ϕ_S	V_{Aa} (km s^{-1})	$(O-C)_{Aa}$ (km s^{-1})	V_{Ab} (km s^{-1})	$(O-C)_{Ab}$ (km s^{-1})	Observatory
44,310.632	0.584	0.268	−25.8	2.0	...	...	HPO
44,313.582	0.586	0.099	37.5	0.0	...	...	HPO
44,340.563	0.602	0.698	−43.8	−1.1	...	...	HPO
44,380.455	0.626	0.933	43.9	0.2	...	...	HPO
44,396.417	0.636	0.428	−84.8	−0.6	...	...	HPO
44,397.445	0.637	0.718	−34.3	0.8	...	...	HPO
44,407.393	0.643	0.519	−91.8	−0.9	...	...	HPO
44,458.354	0.674	0.872	27.6	0.6	...	...	HPO
44,460.354	0.675	0.435	−87.5	−1.1	...	...	HPO
44,461.357	0.676	0.717	−36.2	0.0	...	...	HPO
44,990.753	0.998	0.812	0.4	0.8	...	...	HPO
44,991.734	0.999	0.088	33.2	0.3	...	...	HPO
44,993.755	1.000	0.657	−66.8	−1.0	...	...	HPO
44,994.725	0.000	0.930	37.0	0.2	...	...	HPO
44,995.727	0.001	0.213	−11.0	−0.5	...	...	HPO
45,125.398	0.080	0.732	−32.1	1.0	...	...	HPO
45,126.471	0.081	0.034	42.9	−0.9	...	...	HPO
45,127.417	0.081	0.301	−48.0	−1.0	...	...	HPO
45,410.698	0.254	0.081	41.3	−0.4	...	...	HPO
45,432.598	0.267	0.249	−20.0	−1.0	...	...	HPO
45,433.584	0.268	0.527	−89.0	0.0	...	...	HPO
45,436.566	0.270	0.366	−67.0	−0.5	...	...	HPO
45,437.563	0.270	0.647	−62.6	−0.8	...	...	HPO
45,783.855	0.481	0.174	13.6	−0.6	−69.8	0.8	KPNO
45,813.810	0.499	0.610	−72.2	0.5	71.9	2.9	KPNO
45,814.856	0.500	0.905	39.9	0.2	−107.6[a]	4.6	KPNO
45,852.719[b]	0.523	0.568	−83.0	−0.2	82.4	−2.2	KPNO
46,970.743	0.204	0.438	−85.5	0.8	...	...	KPNO
46,972.741	0.205	0.001	50.6	1.2	...	...	KPNO
47,152.074	0.314	0.507	−89.7	−0.6	...	...	KPNO
47,245.930[b]	0.372	0.940	47.8	0.5	−123.4	0.2	KPNO
47,557.031	0.561	0.555	−85.6	−0.1	86.6	−0.8	KPNO
47,623.904	0.602	0.389	−74.1	−0.1	67.9	1.0	KPNO
47,624.940	0.602	0.681	−50.3	−0.5	29.4	1.6	KPNO
47,625.963	0.603	0.969	48.9	−0.1	−127.5	3.9	KPNO
47,627.919	0.604	0.520	−90.3	−0.3	94.0	1.5	KPNO
48,345.851	0.042	0.712	−43.9	−0.9	−1.0	−2.0	KPNO
48,346.929	0.042	0.015	43.2	−0.8	−139.7	−0.6	KPNO
48,428.802	0.092	0.073	38.6	0.1	−125.0	1.4	KPNO
48,771.839[b]	0.301	0.683	−47.7	−0.1	28.0	0.6	KPNO
48,774.813	0.303	0.521	−88.4	0.3	92.5	−1.2	KPNO
49,101.920	0.502	0.644	−62.4	−0.5	50.4	−1.1	KPNO
49,459.809	0.720	0.437	−88.5	−0.5	81.6	−0.1	KPNO
49,461.928	0.721	0.034	44.9	−1.0	−133.7	0.3	KPNO
49,463.846	0.723	0.574	−86.6	−0.5	79.7	1.3	KPNO
49,834.950	0.949	0.088	32.1	−0.3	−124.7	−0.7	KPNO
49,836.881	0.950	0.632	−75.9	−0.9	49.8	0.7	KPNO
49,900.771	0.989	0.626	−77.2	−0.4	51.4	−1.4	KPNO
49,902.778	0.990	0.191	−1.3	0.2	−66.9	1.6	KPNO
50,198.904	0.170	0.589	−82.2	−0.4	75.8	1.7	KPNO
50,203.855	0.173	0.983	47.9	−0.2	−134.1	0.8	KPNO
50,262.732	0.209	0.565	−85.1	0.5	82.0	−1.3	KPNO
50,266.848	0.212	0.724	−32.7	−0.5	...	...	KPNO
50,578.765	0.402	0.570	−81.8	0.0	85.1	0.3	KPNO
50,631.721	0.434	0.484	−87.9	0.2	94.3	−0.6	KPNO
50,633.720[b]	0.435	0.047	49.2	−0.2	−125.8	0.9	KPNO
50,637.743	0.438	0.180	11.9	−0.2	−65.1	1.4	KPNO
50,832.074	0.556	0.909	39.2	−0.9	−116.0	−1.2	KPNO
50,926.847	0.614	0.601	−76.9	0.3	74.9	3.6	KPNO
51,004.725	0.661	0.533	−90.7	−0.4	88.8	−0.8	KPNO
51,304.894	0.844	0.070	37.6	0.2	−129.6	−0.7	KPNO
51,306.837	0.845	0.618	−78.4	0.0	58.4	0.7	KPNO
51,307.836[b]	0.846	0.899	30.2	−0.2	−116.7	1.0	KPNO
51,348.794	0.871	0.434	−91.0	0.3	76.3	−0.8	KPNO

TABLE 1—*Continued*

Heliocentric Julian Date (HJD − 2,400,000)	ϕ_L	ϕ_S	V_{Aa} (km s^{-1})	$(O-C)_{Aa}$ (km s^{-1})	V_{Ab} (km s^{-1})	$(O-C)_{Ab}$ (km s^{-1})	Observatory
51,657.864	0.059	0.478	−95.3	0.1	87.8	1.1	KPNO
51,659.852	0.060	0.038	42.9	0.0	−135.1	0.9	KPNO
51,732.774	0.105	0.575	−87.2	−0.1	75.6	−1.4	KPNO
51,734.758	0.106	0.133	22.5	−0.4	−98.8	1.4	KPNO
51,803.619	0.148	0.527	−91.8	0.5	89.0	−0.1	KPNO
52,014.930	0.276	0.039	48.8	−0.3	−131.2	−1.7	KPNO
52,329.055	0.468	0.506	−88.1	0.5	95.2	−0.1	KPNO
52,390.845	0.505	0.908	40.5	0.0	−114.0	−0.5	KPNO
52,536.604	0.594	0.958	49.1	1.0	−129.4	0.1	KPNO
52,708.961	0.699	0.499	−92.0	0.9	90.9	−0.2	KPNO
52,758.948	0.730	0.577	−85.8	−0.2	78.1	0.9	KPNO
52,904.592	0.818	0.595	−83.6	0.4	69.4	1.2	KPNO
53,120.894	0.950	0.512	−97.1	0.6	86.4	0.7	KPNO
53,170.730	0.980	0.548	−94.1	0.5	82.9	1.7	KPNO
53,172.852	0.982	0.145	16.2	0.4	−96.4	0.2	KPNO
53,275.590	0.044	0.080	36.3	0.5	−124.6	1.1	KPNO
53,487.735	0.173	0.826	10.6	0.1	−74.8	−0.5	KPNO
53,487.831	0.174	0.853	20.7	0.1	−92.5	−1.9	KPNO
53,487.946	0.174	0.886	31.5	0.5	−108.0	−0.6	KPNO
53,489.816	0.175	0.412	−81.4	0.6	74.1	−0.7	KPNO
53,535.677	0.203	0.328	−54.6	−0.3	31.3	−1.1	KPNO
53,535.767	0.203	0.354	−64.2	−0.4	48.0	0.4	KPNO
53,535.839	0.203	0.374	−70.6	−0.1	59.5	0.9	KPNO

[a] 3 σ residual, velocity given zero weight.
[b] Lithium region, central wavelength 6700 Å.

the observed velocity minus its calculated long-period velocity. Since the orbit is circular, zero phase is a time of maximum velocity of the primary component. Figure 3 presents the velocity curve for the long-period orbit, where zero phase is a time of periastron passage. Each plotted velocity consists of the observed velocity of Aa minus its short-period calculated velocity.

As a matter of interest we obtained three additional solutions. The first allowed the eccentricity of the short-period orbit to vary. The resulting eccentricity, $e = 0.0026 \pm 0.0011$, being just over twice its uncertainty, is not significant, and the application of Bassett's (1978) second test (Lucy 1989) concurred. The second solution included the older DDO velocities of component Aa (Heard 1966) for which a prior analysis of their residuals from the solution in Table 3 indicated individual weights of 0.01 and no observable center-of-mass velocity offset. Because of their low weights, the DDO velocities had little effect on the orbital solution; the long period changed from 1641.6 to 1640.3 days, which is well within the standard error. The third solution incorporated light-time corrections, but their inclusion had no significant effect, so that solution is not presented here.

4. ASTROMETRIC ORBIT

In the *Hipparcos* and Tycho Catalogues (Perryman et al. 1997) HD 131861 is listed as HIP 72939. Unlike most of the stars observed by *Hipparcos*, the successive positions of HD 131861 during the 3 year mission could not be satisfactorily modeled with just five parameters (position, parallax, and proper motion). Instead, a seven-parameter model that included two additional terms for the acceleration, which is the time derivative of the proper motion, was adopted to account for a curvature in the stellar trajectory. As a result, the star is listed in Part G, the Acceleration Solution section, of the Double and Multiple Star Appendix of the *Hipparcos* catalog. A star with such a solution often turns out to have a companion with an orbital period that is too long to be derived from only the *Hipparcos* data. For more information about the *Hipparcos* analysis of such systems see the explanation in § 2.3.1 of the catalog's Volume 1 (Perryman et al. 1997).

Can an orbital solution (Pourbaix & Arenou 2001; Pourbaix & Boffin 2003) advantageously replace the acceleration one? Clearly,

TABLE 2
PHOTOMETRIC OBSERVATIONS OF HD 131861

Heliocentric Julian Date (HJD − 2,400,000)	Var V (mag)	Var R (mag)	Var I (mag)	Chk V (mag)	Chk R (mag)	Chk I (mag)
53,469.0065	1.186	1.078	0.995	−0.972	−1.118	−1.211
53,469.7004	1.199	1.071	1.001	−0.990	−1.107	99.999
53,469.7082	1.181	1.080	0.986	−0.987	−1.111	−1.209
53,469.7143	1.180	1.079	1.010	−0.968	−1.108	−1.204
53,469.7219	1.168	1.096	0.995	−0.965	−1.102	−1.210

NOTES.—Table 2 is published in its entirety in the electronic edition of the *Astronomical Journal*. A portion is shown here for guidance regarding its form and content.

TABLE 3
ORBITAL ELEMENTS OF HD 131861

Parameter	Short Period	Long Period
P (days)	3.55074391 ± 0.00000087	1641.8 ± 2.7
T_0 (HJD)	2,453,271.7567 ± 0.0012	...
T (HJD)	...	2,453,203.0 ± 48.7
γ (km s^{-1})	...	−22.290 ± 0.061
K_{Aa} (km s^{-1})	70.461 ± 0.077	...
K_{Ab} (km s^{-1})	113.52 ± 0.21	...
K_A (km s^{-1})	...	4.731 ± 0.088
e	0.0 (adopted)	0.104 ± 0.017
ω (deg)	...	205.4 ± 11.0
i (deg)	81 ± 2	52 ± 8
Ω (deg)	...	220.0 ± 9.5
a_{Aa} sin i (10^6 km)	3.4404 ± 0.0037	...
a_{Ab} sin i (10^6 km)	5.543 ± 0.010	...
a_A sin i (10^6 km)	...	106.2 ± 2.0
a_A (mas)	...	10 ± 1.4
m_{Aa} sin^3 i ($M_\odot$)	1.4148 ± 0.0059	...
m_{Ab} sin^3 i ($M_\odot$)	0.8782 ± 0.0026	...
$f(m)$ ($M_\odot$)	...	0.0178 ± 0.0010

the *Hipparcos* data did not reveal any astrometric wobble caused by the short-period, 3.55 day system (Jancart et al. 2005). However the long-period, 4.5 yr orbit nicely fits the *Hipparcos* intermediate astrometric data, i.e., the residuals of the solution based on the first five parameters (single-star model) of the adopted *Hipparcos* solution. We used two independent methods to fit the *Hipparcos* observations and determine the orbital parameters. When we adopted the spectroscopic values for the orbital elements P, T, e, K, and ω (Table 3) and reanalyzed the *Hipparcos* data,[4] the agreement between the two sets of parameters was assessed at the 99.9% confidence level. Parameters i, Ω, and a_A from our new astrometric solution are listed in Table 3. Because the original solution, given in the *Hipparcos* catalog (Perryman et al. 1997) only accounted for some curvature, none of the orbital parameters were previously determined.

[4] The *Hipparcos* data are available on the *Hipparcos* catalog CD-ROMs and on the mission Web site at http://www.rssd.esa.int/Hipparcos/InterMedData.html.

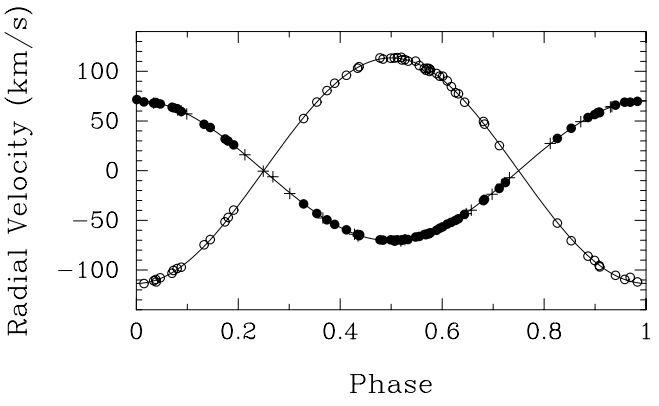

FIG. 2.—Radial-velocity curves of HD 131861 in its short-period orbit. Filled circles represent KPNO velocities, and plus signs represent Coravel velocities of component Aa. Open circles represent KPNO velocities of component Ab. Each plotted velocity represents the observed velocity minus its calculated long-period velocity from the elements in Table 3. The curves represent the short-period elements from the same table. Zero phase is a time of maximum velocity for component Aa.

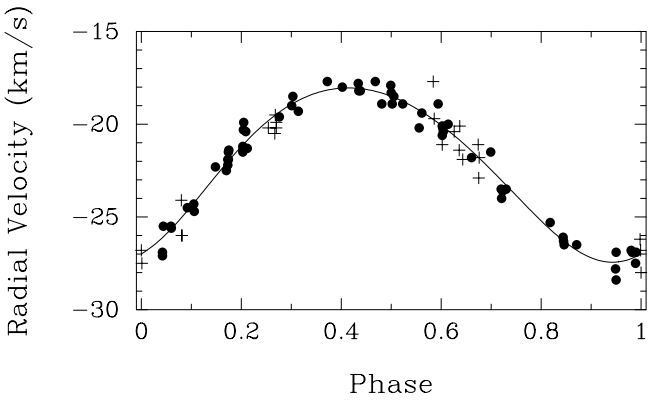

FIG. 3.—Radial-velocity curve of HD 131861 in its long-period orbit. Filled circles represent KPNO velocities, and plus signs represent Coravel velocities. Each plotted velocity is the observed velocity minus the calculated velocity of component Aa in the short-period orbit, calculated from the elements in Table 3. The curve represents the long-period elements from the same table. Zero phase is a time of periastron passage.

To examine the robustness of the astrometric orbit, we computed an additional solution. When only the spectroscopic P, T, and e are imposed on the astrometric data, the derived values for K and ω are within 1 σ of their spectroscopic values, confirming the strong reliability of the astrometric fit. Thus, our adopted orbit, combined with the parallax, yields a radial-velocity semiamplitude that is consistent with the spectroscopic value. Therefore, the orbital inclination and the other parameters from the astrometric solution are very well constrained and should be confirmed once the system is resolved.

The revised parallax of 11.20 ± 0.79 mas is quite consistent with the original *Hipparcos* value of 11.53 ± 0.79 mas, as expected for a system with such a long orbital period. However, the proper motion is severely affected (again, as expected), especially along the declination axis. Instead of −67.5 ± 0.9 and 55.9 ± 0.9 mas yr^{-1} for the proper motions in right ascension and declination, respectively, we now obtain −67.0 ± 1.9 and 63.5 ± 1.5 mas yr^{-1}. The new values are within 1 σ of the Tycho-2 values of −66.2 and 62.1 mas yr^{-1} (Høg et al. 2000).

5. SPECTRAL TYPES, MAGNITUDE DIFFERENCE, AND v sin i

Strassmeier & Fekel (1990) identified several luminosity-sensitive and temperature-sensitive line ratios in the 6430–6465 Å region. Those critical line ratios and the general appearance of the spectrum were employed as spectral-type criteria. However, for stars that are hotter than about early G the line ratios in the 6430 Å region have little sensitivity to luminosity, so only the spectral class of an A or F star can be determined.

Examination of our spectra of HD 131861 in the 6430 Å region shows two sets of broadened lines, components Aa and Ab, but no evidence of lines from a third star, component B (Fig. 1). The spectral type of F5 V (Heard 1965) and the absolute visual magnitude of component Aa computed in § 7 indicate that the primary is a dwarf. Thus, the spectrum of HD 131861 was compared with those of F, G, and early-K dwarfs from the lists of Keenan & McNeil (1989), Fekel (1997), and Gray et al. (2003). Spectra of the reference stars were obtained at KPNO with the same telescope, spectrograph, and detector as our spectra of HD 131861.

With a computer program developed by Huenemoerder & Barden (1984) and Barden (1985), various combinations of reference-star spectra were rotationally broadened, shifted in radial velocity,

appropriately weighted, and added together in an attempt to reproduce the spectrum of HD 131861 in the 6430 Å region. The spectrum of the primary was relatively easy to reproduce with our reference star spectra. However, because the lines of the secondary are quite weak, only 3%–5% deep in the 6430 Å region, stars with a range of spectral types from G5 V to K0 V provided reasonable fits to its spectrum. The best fit to the spectrum of HD 131861 was found with a combination of Procyon, F5 IV–V (Johnson & Morgan 1953) and mean $[\mathrm{Fe/H}] = -0.02$ (Taylor 2003), plus HD 166, G8 V (Gray et al. 2003) and $[\mathrm{Fe/H}] = 0.05$ (Allende Prieto et al. 2004). We thus classify the Aa and Ab components as F5 dwarf and G8: V, respectively, where the colon indicates greater than usual uncertainty in the classification. The iron abundances of the reference stars, used for our best fit, indicate that HD 131861 has an iron abundance quite similar to the Sun's.

The best spectrum-addition fit results in a continuum-intensity ratio of 0.163 for component Ab relative to component Aa. To determine the luminosity ratio of the two components, the intrinsic line-strength ratio must be taken into account, since the actual line strength of the cooler secondary is greater than that of the hotter primary. In the 6430 Å region the average of the Fe I line depths in Procyon relative to those in HD 166 results in a line-strength ratio of 0.662, which we adopt as the Aa/Ab ratio for the components of HD 131861. This produces a luminosity ratio of 0.108, corresponding to a magnitude difference of 2.4 mag in the 6430 Å region. This central wavelength is about 0.6 of the way between the effective wavelengths of the Johnson V and R passbands. Thus, from the mean colors of F5 and G8 dwarfs (Johnson 1966) for the short-period components of HD 131861, we adopt $\Delta V = 2.5$ mag and estimate an uncertainty of 0.4 mag from the various reference-star combinations that were examined. Because the magnitude difference is rather large, its uncertainty affects the apparent magnitude of the secondary much more than that of the primary.

With the procedure of Fekel (1997) we determined projected rotational velocities for the components of HD 131861 from 11 KPNO red-wavelength spectra. For each spectrum the full width at half-maximum of three to five moderate or weak lines of Aa and one or two lines of Ab was measured, and the results were averaged for each component. The instrumental broadening was removed, and the calibration polynomial of Fekel (1997) was used to convert the resulting broadening in angstroms into a total line broadening in km s^{-1}. From Fekel (1997) we assumed a macroturbulence of 4 km s^{-1} for the mid-F dwarf and 3 km s^{-1} for the G dwarf. The resulting $v \sin i$ values are 17 and 15 km s^{-1} for the F5 V and G8 V stars, components Aa and Ab, respectively. The estimated uncertainty for Aa is 1 km s^{-1}. Because the lines of Ab are much weaker than those of Aa, the effects of noise and blends are much greater sources of uncertainty for the $v \sin i$ value of Ab, so we estimate an uncertainty of 3 km s^{-1} for it. In addition, any lines of Aa that happen to blend with Ab will tend to increase the broadening of Ab, so its $v \sin i$ value may be somewhat smaller than our measured value.

6. PHOTOMETRIC ANALYSIS

We were motivated to acquire photometric observations of HD 131861 because the large minimum masses of components Aa and Ab, given in Table 3, strongly suggested that the short-period binary might be eclipsing. Period analyses of our V, R, and I variable-minus-comparison differential magnitudes all produced a very weak signal around 3.5 days. However, plotting the photometric data against those weak photometric periods did not reveal any obvious coherent variability. When we replotted the photometry, phased with the more accurate spectroscopic orbital period (Table 3) and the epoch HJD 2,453,272.6444, which is one-fourth of an orbital cycle after T_0 (Table 3), all three passbands revealed very shallow, grazing primary and secondary eclipses at the correct phases, 0.0 and 0.5, respectively.

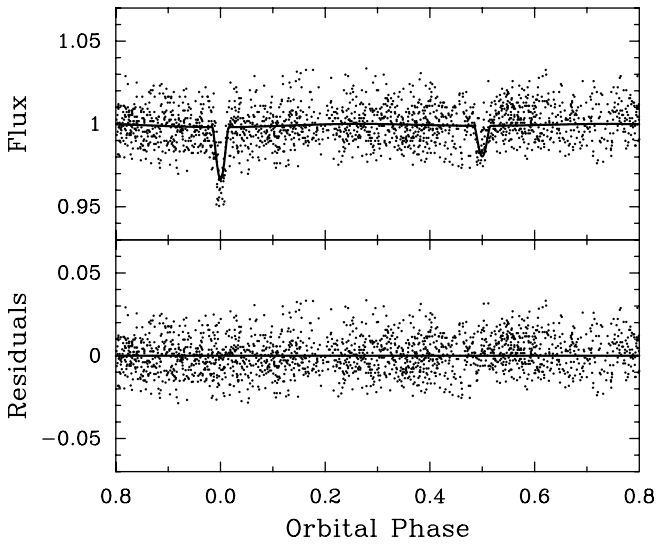

FIG. 4.— *Top:* I-band photometric observations of HD 131861 converted to flux units and plotted vs. orbital phase of the short-period pair. Shallow, grazing primary and secondary eclipses of components Aa and Ab are present. The smooth curve is the best-fit model, with $i = 81\overset{\circ}{.}4$. *Bottom:* Residuals of the light-curve measurements from the best-fit model plotted vs. orbital phase. No unusual systematic deviations of the residuals are seen around primary eclipse, indicating that our model fit to this low-S/N eclipse is satisfactory.

With the eclipse observations removed from the three V, R, and I data sets, the remaining observations scattered about their means with standard deviations of 0.0133, 0.0115, and 0.0120 mag, respectively. This level of precision is not quite as good as the typical precision of 0.006 mag obtained with the T2 telescope because, at $V = 7.9$ mag, HD 131861 is fainter than most targets that this telescope observes. The standard deviations of the check star–minus–comparison star differential magnitudes are 0.0078, 0.0083, and 0.0098 mag in V, R, and I, respectively, consistent with the constancy of both the comparison and check stars. To prepare the three data sets for light-curve modeling, we converted the differential magnitudes to linear flux units with the mean magnitude values (minus the eclipse points) as unity on the flux scales.

Figure 4 (*top*) shows the 1926 I-band flux values plotted against the orbital phase. We modeled the light curve of the short-period binary with the light-curve synthesis software of Bradstreet & Steelman (2002). For a preliminary model we used the minimum stellar masses from Table 3, along with the estimated stellar radii and effective temperatures from Table 4. We also fixed values of the various limb-darkening, gravity-darkening, and reflection coefficients appropriate to the spectral types of the stars and the effective wavelength of the observations. The masses and period were used with Kepler's third law to compute the semimajor axis of the short-period orbit, which, along with the radii, gives the relative radii of the two components. In fitting the light curve we varied only the orbital inclination i, since the S/N of our eclipse photometry is too low to derive other stellar parameters such as the radii and temperatures. The preliminary best-fit solution produced $i = 81^\circ$. We used this initial inclination to convert the minimum masses of Aa and Ab to true masses of 1.47 and 0.91 $M_\odot$,

TABLE 4
FUNDAMENTAL PARAMETERS OF HD 131861

Parameter	Value	Reference
V (mag)	7.91	1
$B - V$ (mag)	0.440	1
Parallax (arcsec)	0.01120 ± 0.00079	2
Spectral type of Aa	F5 V	2, 3
Spectral type of Ab	G8: V	2
$v_{Aa} \sin i$ (km s^{-1})	17 ± 1	2
$v_{Ab} \sin i$ (km s^{-1})	15 ± 3	2
V_{Aa} (mag)	8.01	2
V_{Ab} (mag)	10.51	2
M_V(Aa) (mag)	3.3 ± 0.2	2
M_V(Ab) (mag)	5.8 ± 0.4	2
T_{eff}(Aa) (K)	6587 (adopted)	4
T_{eff}(Ab) (K)	5442 (adopted)	4
L_{Aa} ($L_\odot$)	3.9 ± 0.6	2
L_{Ab} ($L_\odot$	0.5 ± 0.2	2
R_{Aa} ($R_\odot$)	1.5 ± 0.1	2
R_{Ab} ($R_\odot$)	0.8 ± 0.2	2
M_{Aa} ($M_\odot$)	1.47 ± 0.03	2
M_{Ab} ($M_\odot$)	0.91 ± 0.02	2
M_B ($M_\odot$)	0.7 ± 0.1	2

REFERENCES.—(1) Perryman et al. 1997; (2) this work; (3) Heard 1965; (4) Flower 1996.

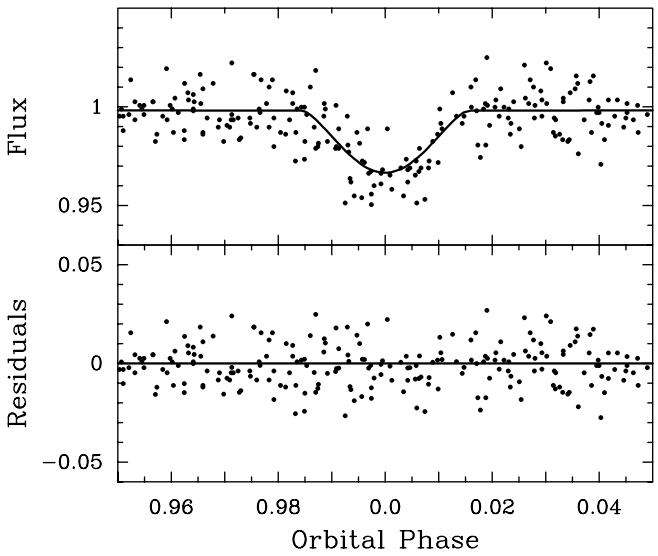

FIG. 5.—*Top:* HD 131861 *I*-band photometric observations around the time of primary eclipse from Fig. 4 replotted with expanded *x*- and *y*-axes. *Bottom:* Corresponding residuals of the light curve from the best-fit model. Again, no unusual systematic deviations of the residuals are seen around primary eclipse.

respectively, given in Table 4. We then repeated the light-curve analyses with the new masses, again varying only the inclination. The resulting inclinations were 81°.4, 81°.3, and 81°.4 for the *V*, *R*, and *I* light curves, respectively. The solid curve in Figure 4 (*top*) is the final computed *I*-band light-curve solution. The reduced χ^2_ν values for the *V*, *R*, and *I* light curves were 1.03, 1.03, and 1.00, respectively, indicating that we have fit the eclipses to the limit of the data precision. However, although the *internal* agreement of our three determinations of i is very good, we estimate the *external* or true uncertainty of i to be 1° or 2°, based on the estimated uncertainty in the stellar temperatures and radii. Our final value of the inclination is given in Table 3 as $81° \pm 2°$.

At first glance, the best-fit light-curve solution in Figure 4 (*top*) appears to be somewhat too shallow at primary eclipse. In Figure 4 (*bottom*) we plot the residuals of the observed light curve from the best-fit solution. No unusual systematic deviations of the residuals are seen around phase 0.0, indicating that our model fit to this low-S/N eclipse is satisfactory. We also replotted the data and best-fit solution around the time of primary eclipse with expanded *x*- and *y*-axes in Figure 5 (*top*) and the corresponding residuals in the bottom panel of that figure. Again, no unusual systematic deviations of the residuals are seen at this scale around phase 0.0.

7. BASIC PROPERTIES

As noted previously, only components Aa and Ab are visible in the spectrum of HD 131861. Nevertheless, it is possible to determine basic properties of the system and its components with the help of our spectroscopic, astrometric, and eclipsing binary orbits.

From the *Hipparcos* catalog (Perryman et al. 1997) the system has $V = 7.91$ mag and $B - V = 0.440$ mag. The ΔV magnitude difference of 2.5 between components Aa and Ab makes component Aa 0.10 mag fainter than the combined magnitude. Thus, a V magnitude of 8.01 and our revised *Hipparcos* parallax of $0''.01120 \pm 0''.00079$ produce $M_V = 3.3 \pm 0.2$ mag. At a distance of 89 ± 6 pc from the Sun, HD 131861 is presumed to be unaffected by interstellar extinction. A $B - V$ value of 0.43, adopted from Johnson (1966), was used in conjunction with Table 3 of Flower (1996) to obtain a bolometric correction and effective temperature for component Aa. Those two quantities in turn were used to compute the luminosity $L = 3.9 \pm 0.6\ L_\odot$ and the radius $R = 1.5 \pm 0.1\ R_\odot$ of component Aa. In a similar manner, for component Ab we determined $V = 10.51$ mag and adopted $B - V = 0.74$ mag. With a resulting $M_V = 5.8 \pm 0.4$ mag this led to luminosity $L = 0.5 \pm 0.2\ L_\odot$ and radius $R = 0.8 \pm 0.2\ R_\odot$ for component Ab. The uncertainty of the effective temperature is estimated to be 200 K for the primary and the secondary. The various quantities are summarized in Table 4. The mass of the long-period companion, component B, can be determined from the total mass of Aa plus Ab, 2.38 $M_\odot$, the long-period orbital inclination derived from our astrometry, 52°, and the mass function of the long-period orbit, 0.0178 $M_\odot$. This combination results in a mass of $0.7 \pm 0.1\ M_\odot$ for component B, producing a mass ratio (Aa + Ab)/B = 3.4.

8. DISCUSSION

8.1. *Lithium Abundance*

From three spectrograms the lithium line, 6707.81 Å, for component Aa has an average equivalent width of 79 mÅ. Correcting for dilution due to the continuum of the secondary produces an equivalent width of 92 mÅ. From Table 2 of Soderblom et al. (1993) this results in a logarithmic lithium abundance of about 3.2. Such a value is similar to the initial lithium abundance found for Population I dwarfs and indicates no significant lithium depletion. It is also consistent with the upper envelope of values found by Balachandran (1990) for about 200 field F stars. There is no clear evidence of a detectable lithium line for component Ab.

8.2. *Synchronization and Circularization*

It is well known (e.g., Tassoul & Tassoul 1996) that tidal interactions affect the rotational and orbital characteristics of close binaries, causing them to tend toward a state in which the rotational axes of the components are parallel to the orbital axis and their rotational velocities are synchronized with the orbital period.

In addition, tidal dissipation of energy causes a binary to circularize its orbit. Indeed, observational results indicate that many close binaries partially or fully accomplish these feats. For stars with convective envelopes Zahn (1977, 1989) investigated the effects of the equilibrium tide on synchronization and circularization, while Tassoul (1987, 1988) explored the theory that binary synchronization and circularization result because of distortions that cause large-scale hydrodynamic currents. Both theories predict that synchronization will occur before circularization.

To determine whether component Aa is synchronously rotating, we combined the orbital period of 3.55 days and the radius of 1.5 $R_\odot$ (Table 4), determined with the Stefan-Boltzmann law, and computed a synchronous rotational velocity of 21.4 km s^{-1}. If the rotational and orbital axes are parallel, as is generally assumed in close binaries, then the rotational inclination is 81°. Since the inclination is so high, we adopt the projected rotational velocity of 17 km s^{-1} as the equatorial rotational velocity. Thus, component Aa is rotating about 20% more slowly than it would if it were synchronously rotating. With an adopted radius of 0.8 $R_\odot$ (Table 4) for component Ab, its computed synchronous rotational velocity is 11.4 km s^{-1}. At face value this indicates that the secondary, with an equatorial rotational velocity of 15 km s^{-1}, is rotating more slowly than synchronous. However, rather large uncertainties in the radius and rotational velocity of Ab make such a conclusion premature. Indeed, as noted in § 5, the projected rotational velocity of Ab may be somewhat overestimated. In addition, our adopted radius is less than the canonical value of 0.88 $R_\odot$ for a G8 V star (Gray 1992). A reduced $v \sin i$ value and increased radius would bring the observed rotational velocity of Ab into better agreement with the synchronous rotational velocity. Thus, component Ab may be synchronously rotating.

As discussed in § 3, the eccentricity of the short-period orbit is extremely small, and we have adopted a zero-eccentricity orbit. However, in triple systems the third star can cause some of the orbital elements of the close pair to vary with time. Changes in the eccentricity have been examined numerically by Mazeh & Shaham (1979) and both analytically and numerically by Söderhjelm (1984). Their results showed that even if the short-period system attained a circular orbit, its eccentricity would be modulated. From Mazeh & Shaham (1979) we computed a modulation period of about 13,000 yr.

8.3. *Orbital Characteristics*

Fekel (1981) compared the short- and long-period orbital inclinations for 20 multiple star systems and found that at least 33% of the orbital pairs are not coplanar. For HD 131861 the long-period orbit has an inclination of 52°. From our photometric solution, the orbital inclination of the short-period binary is 81°. Therefore, it is clear that the short- and long-period orbits are not coplanar.

The total mass of the three stars is 3.08 $M_\odot$. Thus, from Kepler's third law the long-period system has a semimajor axis of 3.96 AU, resulting in an angular separation of 0.″044. The ΔV magnitude difference between the F5 V primary and the presumed mid-K dwarf tertiary is about 4 mag (Gray 1992). However, in the *K*-band of the Johnson system the magnitude difference would decrease by perhaps 2.5 mag (Johnson 1966). So, the only impediment to direct resolution of the long-period system by, for example, the CHARA interferometric array (ten Brummelaar et al. 2003; McAlister et al. 2003) is the faintness of the entire system, $K \sim 6.8$ mag.

This research has been supported at Tennessee State University by NASA grant NCC5-511 and NSF grant HRD 97–06268. D. P. acknowledges support from the European Space Agency via PRODEX research grant 90078. The authors thank the anonymous referee for useful comments.

REFERENCES

Allende Prieto, C., Barklem, P. S., Lambert, D. L., & Cunha, K. 2004, A&A, 420, 183
Balachandran, S. 1990, ApJ, 354, 310
Barden, S. C. 1985, ApJ, 295, 162
Barker, E. S., Evans, D. S., & Laing, J. D. 1967, R. Greenwich Obs. Bull., 130
Barlow, D. J., & Scarfe, C. D. 1991, AJ, 102, 2098
Bassett, E. E. 1978, Observatory, 98, 122
Batten, A. H., Fletcher, J. M., & MacCarthy, D. G. 1989, Publ. Dominion Astrophys. Obs., 17, 1
Bradstreet, D. H., & Steelman, D. P. 2002, BAAS, 34, 1224
Fekel, F. C. 1981, ApJ, 246, 879
———. 1997, PASP, 109, 514
Fekel, F. C., Barlow, D. J., Scarfe, C. D., Jancart, S., & Pourbaix, D. 2005, AJ, 129, 1001
Fekel, F., Jr., Bopp, B. W., & Lacy, C. H. 1978, AJ, 83, 1445
Fitzpatrick, M. J. 1993, in ASP Conf. Ser. 52, Astronomical Data Analysis Software and Systems II, ed. R. J. Hanisch, R. V. J. Brissenden, & J. Barnes (San Francisco: ASP), 472
Flower, P. J. 1996, ApJ, 469, 355
Gray, D. F. 1992, The Observation and Analysis of Stellar Photospheres (Cambridge: Cambridge Univ. Press)
Gray, R. O., Corbally, C. J., Garrison, R. F., McFadden, M. T., & Peterson, P. E. 2003, AJ, 126, 2048
Heard, J. F. 1965, Publ. David Dunlap Obs., 2, 443
———. 1966, J. R. Astron. Soc. Canada, 60, 128
Henry, G. W. 1995a, in ASP Conf. Ser. 79, Robotic Telescopes: Current Capabilities, Present Developments, and Future Prospects for Automated Astronomy, ed. G. W. Henry & J. A. Eaton (San Francisco: ASP), 37
———. 1995b, in ASP Conf. Ser. 79, Robotic Telescopes: Current Capabilities, Present Developments, and Future Prospects for Automated Astronomy, ed. G. W. Henry & J. A. Eaton (San Francisco: ASP), 44
Høg, E., et al. 2000, A&A, 365, L27
Huenemoerder, D. P., & Barden, S. C. 1984, BAAS, 16, 510
Jancart, S., Jorissen, A., Babusiaux, C., & Pourbaix, D. 2005, A&A, 442, 365
Johnson, H. L. 1966, ARA&A, 4, 193
Johnson, H. L., & Morgan, W. W. 1953, ApJ, 117, 313
Keenan, P. C., & McNeil, R. C. 1989, ApJS, 71, 245
Lucy, L. B. 1989, Observatory, 109, 100
Mayor, M., & Mazeh, T. 1987, A&A, 171, 157
Mazeh, T., & Shaham, J. 1979, A&A, 77, 145
McAlister, H. A., et al. 2003, Proc. SPIE, 4838, 476
Perryman, M. A. C., et al. 1997, The *Hipparcos* and Tycho Catalogues (ESA SP-1200; Noordwijk: ESA)
Pourbaix, D., & Arenou, F. 2001, A&A, 372, 935
Pourbaix, D., & Boffin, H. 2003, A&A, 398, 1163
Scarfe, C. D., Batten, A. H., & Fletcher, J. M. 1990, Publ. Dominion Astrophys. Obs., 18, 21
Soderblom, D. R., Jones, B. F., Balachandran, S., Stauffer, J. R., Duncan, D., Fedele, S. B., & Hudon, J. D. 1993, AJ, 106, 1059
Söderhjelm, S. 1984, A&A, 141, 232
Strassmeier, K. G., & Fekel, F. C. 1990, A&A, 230, 389
Tassoul, J.-L. 1987, ApJ, 322, 856
———. 1988, ApJ, 324, L71
Tassoul, J.-L., & Tassoul, M. 1996, Fundam. Cosmic Phys., 16, 377
Taylor, B. J. 2003, A&A, 398, 731
ten Brummelaar, T. A., et al. 2003, Proc. SPIE, 4838, 69
Wolfe, R. H., Horak, H. G., & Storer, N. W. 1967, in Modern Astrophysics, ed. M. Hack (New York: Gordon & Breach), 251
Zahn, J.-P. 1977, A&A, 57, 383
———. 1989, A&A, 220, 112